Ground-based measurements of total ozone column amount with a multi-channel moderate-bandwidth filter instrument at the Troll Research Station, Antarctica

MILOS SZTIPANOV[1*], LUBNA TUMEH[2], WEI LI[1], TOVE SVENDBY[3], ARVE KYLLING[3], ARNE DAHLBACK[4], JAKOB J. STAMNES[5], GEORG HANSEN[3], KNUT STAMNES[1]

[1]*Stevens Institute of Technology, Department of Physics, Light and Life Laboratory, 1 Castle Point Terrace, Hoboken, NJ 07030, USA*
[2]*Manhattan College, 4513 Manhattan College Pkwy, The Bronx, NY 10471, USA*
[3]*NILU, Instituttveien 18, 2007 Kjeller, Norway*
[4] *University of Oslo, Problemveien 7, 0315 Oslo, Norway*
[5] *University of Bergen, 5007 Bergen, Norway*
[*]*msztipan@stevens.edu*

Abstract: Combining information from several channels of the NILU-UV (Norwegian Institute for Air Research - Ultraviolet) irradiance meter, one may determine the total ozone column (TOC) amount. A NILU-UV instrument has been deployed and operated on two locations at Troll research station in Jutulsessen, Queen Maud Land Antarctica for several years. The method used to determine the TOC amount is presented and the derived TOC values are compared with those obtained from the Ozone Monitoring Instrument (OMI) located on NASA's AURA satellite. The findings show that the NILU-UV TOC amounts correlate well with the results of the OMI and that the NILU-UV instruments are suitable for monitoring the long-term change and development of the ozone hole. Because of the large footprint of OMI, NILU-UV is a more suitable instrument for local measurements.

1. Introduction

Solar radiation (directly or indirectly) fuels all life on Earth. It plays a major role in the original synthesis of biomolecules, photosynthesis, and in the evolution of life. Ultraviolet (UV) radiation reaching the surface of the Earth (~280–400 nm) is a biologically significant and important part of the solar spectrum. The solar UV spectrum itself is divided into sub-regions. Our interest focuses on the UVB (280–315 nm) and UVA (315–400 nm) regions. Electromagnetic radiation in the UVB spectral range can have serious biological effects on living organisms and biomolecules. Many acute and chronic health damages to the skin, eyes, and the immune system can be caused by UV radiation [1, 2]. Furthermore, degenerative changes in cells as well as damages in DNA and chromosomes can be caused by exposure to UV radiation [3–7]. The most well known problems caused by high doses of UV radiation are: sunburn, skin aging, skin cancer, inflammatory reactions in the eyes, and cataracts.

At the same time, exposure of the skin to a small amount of UV radiation is sufficient to produce vitamin-D in an efficient manner. Vitamin-D is essential in strengthening the immune system, reducing the risk of various cancers, heart diseases, immune disorders and in alleviating depression [2, 6]. Atmospheric ozone absorbs UVB radiation and thereby protects the biosphere; the total sum of living organisms (including ecosystems and humans). The stratosphere contains about 90% of the total ozone column, which varies with location and time.

The region on Earth where the ozone depletion due to human pollution is most extreme

and variable, is situated above Antarctica. It is evident that the total ozone column (TOC) amount is an important quantity in our biosphere and that changes in the ozone layer can be closely monitored by quantifying the TOC amount. The status of the ozone layer in Antarctica has been monitored since 1957 [8] using several types of instruments, including scanning spectroradiometers, multi-channel narrow–bandwidth, moderate–bandwidth, and single-channel broad–bandwidth filter instruments. Monitoring has also been done remotely from satellites. Ground-based instruments look at the atmosphere from the surface and provide a completely independent measurement of the TOC amount that can be compared with satellite measurement. This ground-based capability has proven very useful in the past. Very low TOC values observed over the Antarctic region were not reported by NASA's satellite teams because these low values were thought to be due to instrument degradation or malfunction [9]. Initially these very low TOC values were believed simply to be unreliable until similar low TOC values derived from ground-based instruments were published [10]. The different types of instruments have their pros and cons depending on the accessibility of the measurement site, accuracy, stability, environment, quality requirements, manpower, and financial resources. An accurate, reliable instrument that could operate on its own in harsh conditions would be a very useful tool.

In this study, TOC amounts derived from data collected by NILU-UV irradiance meters over twelve years have been analyzed and compared with TOC amounts derived from data collected by the Ozone Monitoring Instrument (OMI) deployed on NASA's AURA satellite [11]. Besides documenting and discussing the variations in the ozone layer observed over this site, the goal of this research is also to examine possible reasons for discrepancies between TOC amounts inferred from the ground-based NILU-UV instrument and the satellite-deployed OMI instrument.

2. Instrumentation

2.1. The NILU-UV Instrument

The NILU-UV radiometer is a ground-based filter instrument with five UV channels at wavelengths centered around 302, 312, 320, 340, and 380 nm. The bandwidth is $\sim$ 10 nm at full width at half maximum (FWHM). A sixth channel takes measurements in the visible (or so-called photosyntetically active) range, 400–700 nm with a bandwidth of 300 nm at FWHM. The front optics of the device has a Teflon diffuser, followed by interference filters, and each channel is equipped with UG-11 bandpass optical glass filters. In addition, the channels 302, 312, and 320 nm are equipped with shortpass filters to transmit light at wavelengths shorter than the cut-off wavelength and reject light at longer ones. The radiometer has built-in memory to store data and a temperature controller. It records data at a 1-minute time resolution. Besides the (limited capacity) built-in memory, data can be recorded and stored by connecting the device to a computer with a RS-232 port. The instrument is equipped with moderate bandwidth filters that tend to drift with time; hence the instrument requires a relative calibration (typically once or twice a month). Based on the log files of the instrument (deployed at Troll-Station Antarctica) it had been calibrated once a month. The total weight of the instrument is 3.3 kg; it is waterproof and designed to operate in harsh environments.

During the measurements two different locations and two NILU-UV instruments were used. From January 27, 2007 until May 11, 2015 instrument number 015 was deployed, first at location $-72.01°$S, $2.323°$E, until January 19, 2014. Measurements restarted in January 30, 2014 at a new location, $-72.01°$S, $2.535°$E, Trollhaugen. Due to a technical issue the reliability of the data from this instrument from January 2015 dropped. The measurements with instrument 015 finally stopped on May 11, 2015. In the following sections, the 2015 measurements are marked in gray to indicate their unreliability. A new instrument (number 005) was installed on November 24, 2015 at the Trollhaugen location and has been operating ever since.

2.2. The OMI

The Ozone Monitoring Instrument (OMI) is deployed on NASA's AURA satellite which is in a Sun-synchronous orbit. This satellite was launched on July 15, 2004. The OMI is measuring TOC amounts, UV-radiation, and aerosol abundance. OMI data are gridded at 0.25 degrees, it has a 780 × 576 (spectral × spatial) pixel CCD detector. AURA's swath is 2600 km and the nadir viewing footprint is 13 km × 24 km.

3. Calibrations

3.1. Absolute Calibration

As a NILU-UV instrument gets illuminated hemispherically, the photodetector transforms the radiation to electric current. The current flow from the detectors are measured and subsequently converted to a voltage that is recorded by the instrument processor.

The measured voltage in channel i is:

$$V_i = k_i \int_0^\infty R_i'(\lambda) F(\lambda) d\lambda \tag{1}$$

where k_i is a constant, $R_i'(\lambda)$ is the relative spectral response function for channel i and $F(\lambda)$ is the solar irradiance at wavelength λ. To ensure that the calibration is as accurate as possible the Sun is used as the light source. The irradiance $F(\lambda)$ was measured by a reference radiometer at the same time and location as NILU-UV was recording the voltage V_i. The relative spectral response function for each NILU-UV was characterized at the optical laboratory of the Norwegian Radiation and Nuclear Safety Authority (Direktoratet for strålevern og atomsikkerhet, DSA) When one knows the information above, one can calculate the constant k_i as follows:

$$k_i = \frac{V_i}{\int_0^\infty R_i'(\lambda) F(\lambda) d\lambda}. \tag{2}$$

Once k_i values have been calculated, the voltages can be converted into $F(\lambda)$ irradiances by Eq. (1). Both instrument 015 and 005 were calibrated by DSA. NILU-UV instrument number 015 was calibrated on June 27, 2005 at 1120 (UTC), and instrument 005 was calibrated on August 22, 2015 at 1113 (UTC).

Note, that because the shape of the solar spectrum at the surface depends on the solar zenith angle (SZA) and the TOC amount, the spectral distribution of $R_i'(\lambda)F(\lambda)$ in Eq. (1) will depend on these parameters [12]. The error in the measured irradiance for a channel depends on how much the atmospheric conditions at the time of the measurement differ from those at the time of the absolute calibration.

3.2. Relative Calibration

Relative calibrations are needed at regular time intervals to determine the drift factor which is used to compensate for the degradation of the optical components. The relative calibrations took place at the Troll research station (see Fig. 1) once every month. The calibration setup includes a computer, a stand and a hood for the instrument, three light bulbs, two power-supplies, and a multimeter.

In each channel the voltages are measured for the three different light sources. For each bulb the ratio between the measured voltage and the corresponding voltage recorded in the first calibration is calculated. The average of these three ratios is defined as the relative calibration coefficient (RCC_i), which is used to correct the measurements against drifts.

$$\mathrm{RCC}_i = \frac{1}{3}\left(\frac{V_{m1}}{V_{i1}} + \frac{V_{m2}}{V_{i2}} + \frac{V_{m3}}{V_{i3}}\right). \tag{3}$$

Here V_{m1}, V_{m2}, and V_{m3} are the measured voltages for the three lamps and V_{i1}, V_{i2}, and V_{i3} are the corresponding voltages recorded in the relative calibration initially, right after the absolute calibration.

Channel 6 (400-700 nm), is typically very stable over time. Therefore if one lamp shows unexpected large drift in this channel, it indicates problems with the particular lamp itself. In the case of instrument 015 lamp 1 and 3 showed such behaviors. In order to overcome this problem lamp 2 was used for drift calculations.

4. Methodology

4.1. NILU-UV

When solar radiation passes through the ozone layer of the atmosphere, a portion of the UVB radiation will be absorbed by ozone, while the portion that penetrates the ozone layer will be multiply scattered or absorbed by air molecules, aerosols, and cloud particles [13]. To take into account the effects of clouds, aerosol particles, and surface albedo on the UV radiation a *radiation modification factor* (RMF) or *cloud transmission factor* (CLT = RMF × 100) is introduced. The RMF is the measured irradiance at wavelength λ and solar zenith angle θ_0, $F_m(\lambda, \theta_0, \mathrm{TOC})$, divided by the calculated irradiance, $F_c(\lambda, \theta_0, \mathrm{TOC})$, at the same λ and θ_0 at the altitude of the site for a cloud- and aerosol-free sky and zero surface albedo.

$$\mathrm{CLT} = \mathrm{RMF} \times 100 = \frac{F_m(\lambda, \theta_0, \mathrm{TOC})}{F_c(\lambda, \theta_0, \mathrm{TOC})} \times 100. \tag{4}$$

In this study the 340 nm channel was used to determine the CLT. The CLT defined here is not sensitive to ozone because its absorption cross section is very small at $\lambda = 340$ nm, whereas the CLT is sensitive to clouds, aerosol particles, and the surface albedo. CLT may be larger than 100 when broken clouds are present and the direct beam from the unobscured Sun is measured by the instrument as well as diffuse sky radiation scattered by broken clouds. Furthermore, snow on the ground enhances the albedo and thus the radiation reflected from the surface. Such a circumstance will increase the downward irradiance and may give CLT values larger than 100 [14].

The TOC amount can be determined from spectral global UV irradiance measurements by comparing the measured and calculated N values derived from a Radiative Transfer Model (RTM) [15]. Here N is defined as the ratio of irradiances in two different UV channels, with spectral response functions $R_i(\lambda)$ and $R_j(\lambda)$. One of the channels is sensitive to the TOC amount, while the other is not, or significantly less sensitive. Hence, the N value is defined as:

$$N(\theta_0, \mathrm{TOC}) = \frac{\sum_{\lambda=0}^{\infty} R_i(\lambda) F(\lambda, \theta_0, \mathrm{TOC})}{\sum_{\lambda=0}^{\infty} R_j(\lambda) F(\lambda, \theta_0, \mathrm{TOC})} \tag{5}$$

where $F(\lambda, \theta_0, \mathrm{TOC})$ is the spectral irradiance, λ is the wavelength, and θ_0 is the solar zenith angle. In this research the ratio $\frac{channel2}{channel1}$ was used to calculate N in Eq. (5). A radiative transfer model (RTM) was used to quantify how the radiation is affected by ozone absorption and other constituents (Rayleigh scattering by the bulk density of molecules and scattering/absorption by cloud/aerosol particles) in the atmosphere. To create a table of $N(\theta_0, \mathrm{TOC})$ values as a function of θ_0, TOC, and latitude, a RTM based on the discrete ordinate method was used as described by Dahlback [12]. The TOC value can be inferred by comparing the measured $N(\theta_0, \mathrm{TOC})$ with the calculated one.

4.2. OMI

Details about OMI's TOC retrieval algorithm (version 8.5) are available in the Algorithm Theoretical Basis Documents [16]. The TOC retrieval method uses backscattered radiances in two channels. For $\theta_0 < 80°$, the channels are centered at 317.5 and 331.2 nm. For $\theta_0 > 80°$ the channels are centered at 331.2 and 360 nm. For all SZA the shorter wavelength is used to retrieve the TOC values. To improve the accuracy, the impact of cloud cover on the backscattered radiation is estimated using the longer wavelength for all SZA.

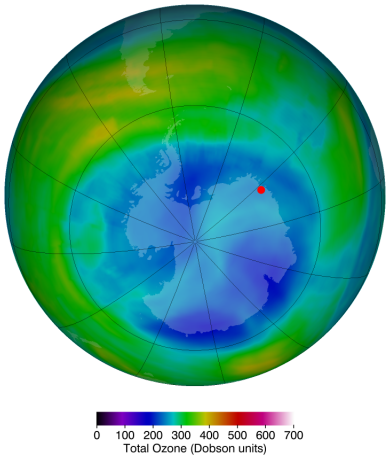

Fig. 1: False-color view of total ozone over the Antarctic pole on August 29, 2015. The purple and blue colors indicate the smallest amounts of ozone, and the yellow and red colors indicate relatively larger mounts of ozone. The location of the Troll Research Station is indicated by the red dot. (Original figure created by NASA [17].)

5. Measurements and data analysis

The measurements took place at Troll Station, Jutulsessen, Queen Maud Land Antarctica (−72.01°S, 2.323°E, alt:1275 m and −72.01°S, 2.535°E, alt:1553 m). As shown in Fig. 1(Original figure created by NASA, based on data obtained from OMI), this location is frequently under the ozone hole. Measurements were made between 2007 and 2018. Version 2.0 of the NILU-UV Data Processing software [18] was used to determine the TOC amounts by the look up table method. In this study the ratio between irradiances measured in channel 2 (312 nm) and channel 1 (302 nm) was used to determine the TOC. Fan et al. [19] showed that cloud cover (quantified by the CLT value) will affect the relative difference between the TOC retrieved from OMI data and the TOC obtained from NILU-UV data. The difference starts to increase when the CLT becomes smaller than 65. For cloud-free conditions and SZA $< 70°$ the overall uncertainty is estimated to be ±5% [15, 20]. For SZA $> 70°$ the impact of cloudiness, the vertical profile of ozone and temperature, the imperfect cosine response of the instrument, and the absolute calibration error reduce the accuracy of the results [21]. A one-hour average of TOC around local noon (CEST, Central European Summer Time: March-October, UTC+0 DST, Daylight Saving Time: October-March) was taken. Because of the above-mentioned limitations, the ozone averages contain minute by minute measurements for CLT > 30 and SZA $< 80°$.

6. Results

The daily average TOC values derived from the NILU-UV measurements are plotted versus the day of the year. Figures 2a and 3a show the daily averages of TOC amounts of NILU-UV and

OMI on the same graph for years 2010 and 2013. Similar plots were made for years from 2007 until the end of 2018 (see Appendix 9).

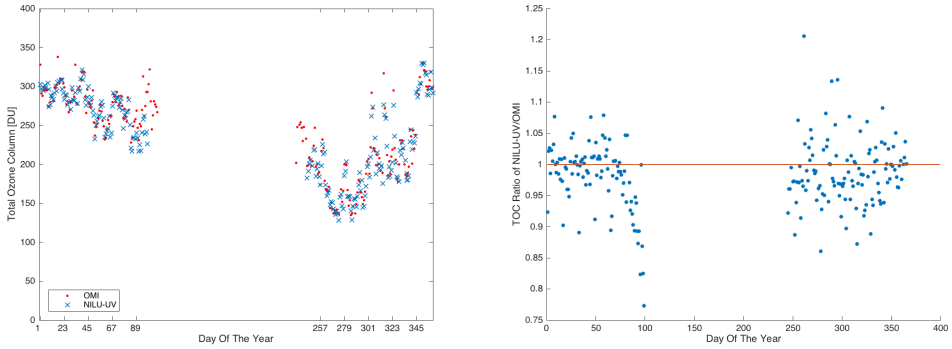

(a) TOC values from OMI (red dots) and NILU-UV (blue crosses) vs. day of the year for 2010.

(b) The ratios between TOC values derived from NILU-UV and OMI vs the day of the year for 2010.

Fig. 2

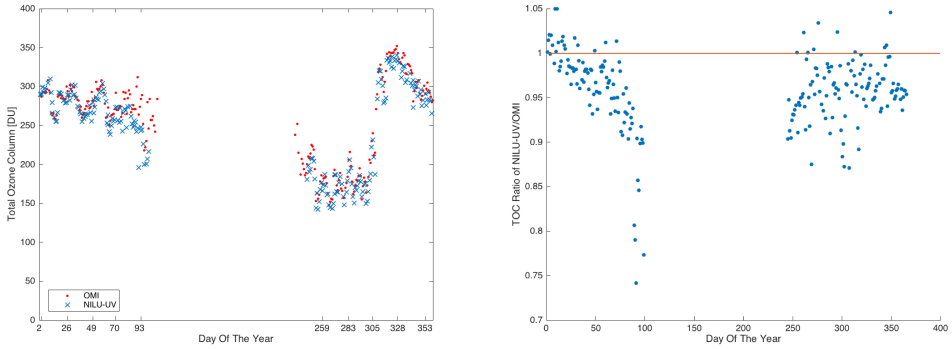

(a) TOC values from OMI (red dots) and NILU-UV (blue crosses) vs. day of the year for 2013.

(b) The ratios between TOC values derived from NILU-UV and OMI vs the day of the year for 2013.

Fig. 3

All the plots show the same behavior, that is, the TOC values retrieved from NILU-UV tend to be lower than the corresponding OMI values. To examine this tendency the TOC amounts measured by NILU-UV was divided by the amounts measured by the OMI and the ratio ($\frac{NILU-UV}{OMI}$) of these values were plotted. The results are shown in Figures 2b and 3b. A horizontal line where the ratio equals one is included in these figures.

From Figures 2b and 3b it is evident that as the day of the year (DOY) is getting closer to the Antarctic winter the ratio of NILU-UV/OMI flips and NILU-UV measures higher values than OMI. This behavior might indicate a SZA related error either in NILU-UV or OMI measurements.

Taking the OMI results as a reference and using the daily averages from NILU-UV, the absolute and relative differences as well as the average absolute value of these quantities were calculated for yearly periods as follows (here x refers to the TOC value):

$$d_a(x, x_{ref}) = x_{ref} - x \tag{6}$$

$$d_r(x, x_{ref}) \equiv \frac{x_{ref} - x}{x_{ref}} \times 100 \tag{7}$$

$$|d_a(x, x_{ref})| = |x_{ref} - x| \tag{8}$$

$$|d_r(x, x_{ref})| \equiv \frac{|x_{ref} - x|}{x_{ref}} \times 100. \tag{9}$$

The absolute and relative differences, given by Eqs. (8) and (9), provide a quantitative measure of how far the different data points are from each other or relative to each other. Even if there were more data points per year for NILU-UV than for OMI (or vice versa), differences can only be calculated for corresponding days. Note that the computed mean values of the differences calculated by using Eqs. (8) and (9) were higher than the mean of the absolute and relative differences calculated by Eqs. (6) and (7). This result is a direct consequence of how the differences were defined. The absolute and relative differences computed by Eqs. (8) and (9) for all years (2007–2018) are provided in Table 1. Presumably, the years 2013 and 2014 show higher differences due to instrument degradation.

Table 1: Statistical results for years 2007-2018.

Data	**Ave.Rel.Dif. [%]**	**Ave.Abs.Dif. [DU]**	**|Ave.Rel.Dif.| [%]**	**|Ave.Abs.Dif.| [DU]**
2007	1.23	2.76	4.56	10.04
2008	2.18	4.87	4.29	9.63
2009	3.09	7.86	4.45	10.90
2010	1.61	4.29	3.95	9.40
2011	0.56	1.90	3.51	7.68
2012	1.29	3.62	3.82	9.48
2013	4.18	10.63	4.58	11.69
2014	6.32	14.86	6.60	15.43
2015	8.75	22.97	8.87	23.25
2016	0.91	0.55	4.18	9.14
2017	-1.51	-4.69	4.02	10.17
2018	-2.65	-7.73	5.07	12.25
std	2.47	6.37	0.83	2.05

To examine how reliable the NILU-UV instrument is for ozone hole monitoring, the yearly average TOC values of the ozone hole above the site, for 2007-2018 are plotted in Fig. 4. The original figure, not including the NILU-UV measurement results, was created by NASA [8]. In Fig. 4, the NILU-UV results clearly correlate with the other measurements.

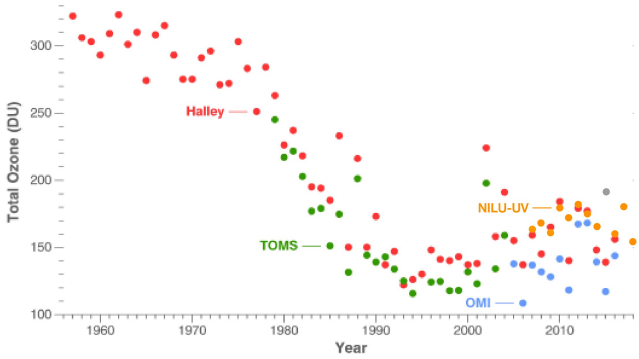

Fig. 4: Comparison of ozone hole measurements, from the ground (at Halley Bay and Troll (NILU-UV) stations) and from space (the Total Ozone Mapping Spectrometer [TOMS] and OMI).

It has been conjectured [22] that a total column ozone level of less than 220 DU is the result of catalyzed ozone loss from chlorine and bromine compounds. Hence, the 220 DU level may be used as a boundary of the region representing ozone loss [22]. For these reasons, yearly ozone hole averages were calculated during the Antarctic Spring for all days when the daily TOC average was equal to or less than 220 DU. The mean TOC amounts so determined are provided in Table 2 and shown in Fig. 4. The differences between the yearly mean and the ozone-hole average values are shown in Fig. 5 for the NILU-UV measurements obtained at the Troll station.

Table 2: Yearly mean ozone hole values from NILU-UV.

Year	**Ave. O_3[DU]**
2007	163.8
2013	175.3
2008	168.6
2014	165.8
2009	161.0
2015	191.6
2010	179.6
2016	160.1
2011	172.7
2017	180.5
2012	182.3
2018	154.4

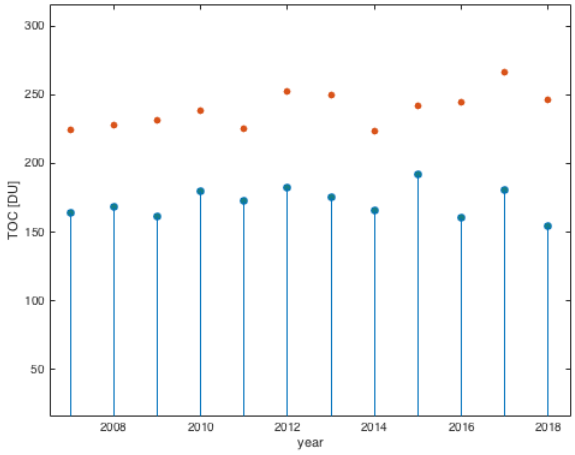

Fig. 5: Average yearly TOC amounts (red dots) and ozone-hole averages (blue dots) derived from NILU-UV measurements between 2007 and 2018.

There are multiple instrumental, environmental, and configurational reasons that may have contributed to discrepancies between the NILU-UV and OMI results. The absolute calibration method of the NILU-UV can also play a role for reasons mentioned in Section 3.1. Another possible cause for errors can arise because for instrument 015 the first relative calibration was on day 122, 2007, which means that about 2 years passed between the absolute calibration and the first relative calibration. The instrument was not exposed to UV radiation and kept at room temperature in that time period. Possible environmental causes could be: dirt, snow or ice cover on the instrument, and extreme temperatures. Although the calculation of TOC amounts uses the ratio between two channels which tend to cancel out cloud effects, for optically thick clouds the accuracy decreases [19]. Dahlback [12] showed that for clouds located between 2 and 4 km with an optical depth of $\tau = 100$ at zero surface albedo the error in the calculated TOC is less than 2 DU compared with the TOC obtained for a cloudless sky. The error will increase if the surface albedo increases. In the presence of a cloud between 2 and 4 km with optical depth $\tau = 100$ and a surface albedo of 0.8 the error is larger, but will not exceed 20 DU. At $\tau = 50$ and surface albedo of 0.8 NILU-UV underestimates the TOC by $\sim 6\%$ [14]. Because of the mixture of soil, rock, and snow covering the surface at the Troll site, the influence of the surface cannot be ruled out.

Differences between TOC amounts obtained from satellite sensors and from ground-based Brewer and Dobson instruments are typically smaller than $\pm 2 - \pm 3\%$ at northern mid-latitudes but become larger at higher latitudes [14]. These percentages are not directly comparable with those obtained from the NILU-UV, but they give qualitative information about the accuracy to be expected when deriving TOC amounts from measurements with different instruments in current use [23].

The ozone layer above Antarctica can be highly varying by time and location. Above such a region, the large footprint (see Section 2.2) of a satellite instrument, like the OMI, can cause considerable discrepancies between OMI and NILU-UV measurements. In Antarctic autumn, there is less spatial ozone variability resulting in a more compact distribution, while the variability is larger under ozone hole conditions in spring, causing more scattering of the deviations, as seen in Fig. 2b.

7. Discussion

In general we can say that the NILU-UV measurements are consistent year by year, showing similar patterns and following the same tendencies as results from the OMI (see Figs. 2a and 3a and more in Appendix 9).

A year-by-year analysis of the NILU-UV data has also been done. Chlorine atoms are responsible for the rapid destruction of ozone. As ultraviolet light is needed to break the bond holding chlorine atoms to the chlorofluorocarbon molecules present in the stratosphere, it is clear that sunlight is needed to trigger the chemical reactions. After the Antarctic winter the NILU-UV instrument data were used from the day of the year (DOY) 245 (September 2), which is the first day of the year when around solar noon the SZA reaches values below 80°. As described in Section 5 NILU-UV data were used when the SZA was smaller than 80°. This is around 35 days after the Sun appears following the Winter darkness and the decline of the TOC amount begins around this time of the year. The year-by-year findings are provided in Tables 3 and 4. For reasons mentioned in Section 2.1 NILU-UV data from 2015 are either unavailable or unreliable. In both Tables 3 and 4 the data for 2015 are marked grey as an indication, that they are based on OMI data.

Table 3: Yearly overview of the ozone hole based on NILU-UV data. (The results for 2015 are from OMI data).

Year	Duration [days]	Yearly Min. [DU]	DOY Of Min.
2007	101	120.5	278
2008	108	115	276
2009	69	112.6	274
2010	97	128.2	274
2011	102	126.1	266
2012	62	149	264
2013	63	142	255
2014	90	123.1	275
2015	106	124	292
2016	76	88.5	274
2017	68	141.9	282
2018	79	121.7	310

Table 4: Yearly overview of the start and end day of the ozone hole. (The results for 2015 are from OMI data).

Year	Beginning	End
2007	245	345
2008	274	352
2009	245	313
2010	245	341
2011	245	346
2012	246	307
2013	245	307
2014	245	334
2015	245	350
2016	246	321
2017	247	314
2018	245	323

In 2010, NILU-UV measurements show that the ozone hole period was between DOY 245 and 341, i.e., from September 2 until December 07, with a total number of 97 days. Towards the end of the ozone hole period there were a few days when the TOC amount slightly exceeded the 220 DU value (see Fig 6. In 2016 the ozone hole period lasted 76 days, starting on day 246 and ending on day 321. Excluding the outlier on day 274 with the value of 88.5 DU, the minimum TOC amount was 125 DU on day 273 (see Fig. 7). For the entire 12-year period of observations, the lowest TOC value was found to occur between days 255 and 310 with the average of day 275 (excluding results from 2015).

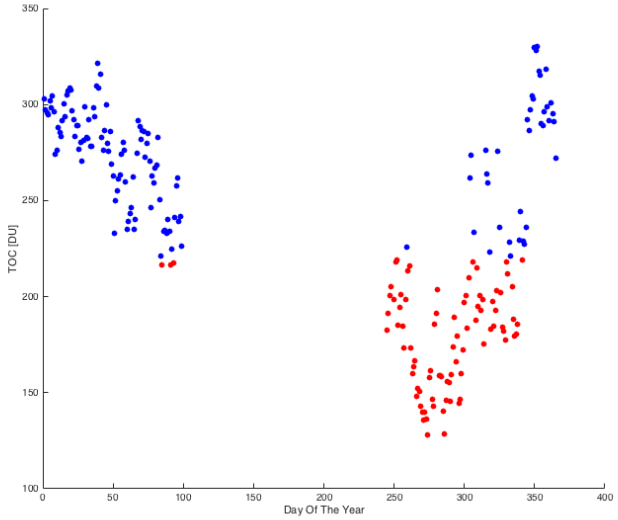

Fig. 6: Ozone hole in 2010. The red dots represent TOC values less than 220 DU.

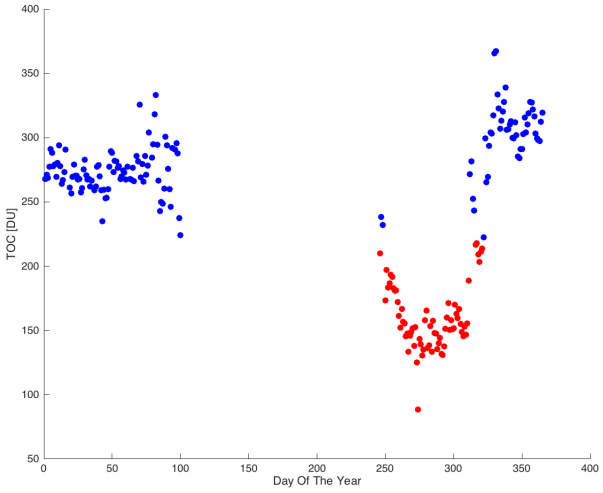

Fig. 7: Ozone hole in 2016. The red dots represent TOC values less than 220 DU.

An observation about the duration of the ozone hole and the shape of the TOC amount curves can be made. For seven out of the twelve years considered in this study, the duration of the ozone hole was significantly shorter (under 100 days) than for the remaining five years when it was about or above 100 days. These five years of short duration are: 2007, 2008, 2010, 2011, and 2014. A specific feature is discernible in the plots for these years (see Figs. 9 a, b, c, d and e). Between the beginning and end of the ozone hole period there is always an up rise, a small peak in the TOC amount. These peaks in years (2009, 2012, 2013, 2015, 2016, 2017, 2018), when the ozone hole period was shorter, are either not present or significantly lower and shifted to the

right, closer towards the end of the period (see Figs. 10, 11, 3a). These peaks are also apparent in the OMI data. This effect is caused by the dynamics of the ozone hole. When it is the shrinking period of the ozone hole, the shape of the hole varies [24]. The above mentioned phenomena typically occurs during November i.e. the location of the NILU-UV instrument is near the border of the ozone hole and it gets in and out of the hole (see Fig. 8).

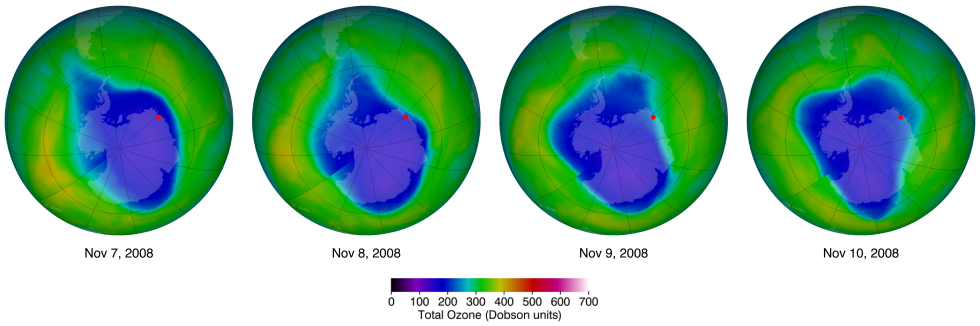

Fig. 8: Troll research station on the border of the ozone hole in 2008 November.

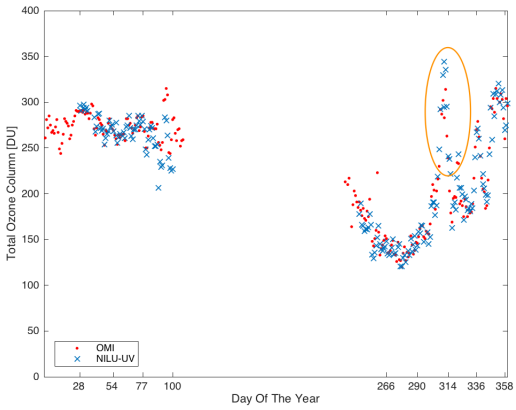

Fig. 9: a. Uprise between the beginning and end of the ozone hole period. TOC values from OMI (red dots) and NILU-UV (blue asterisks) vs day of the year (DOY) in 2007.

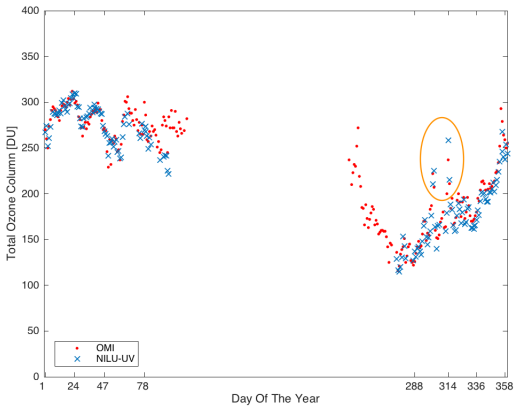

b. TOC peak in 2008.

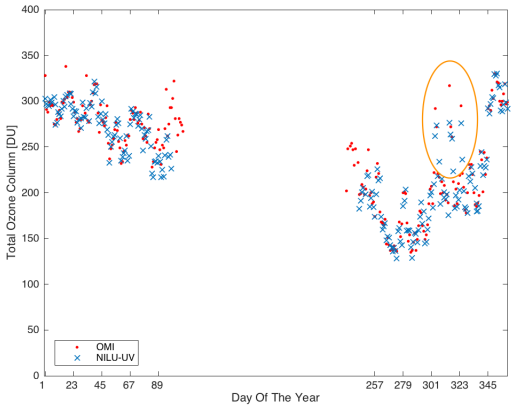

c. TOC peak in 2010.

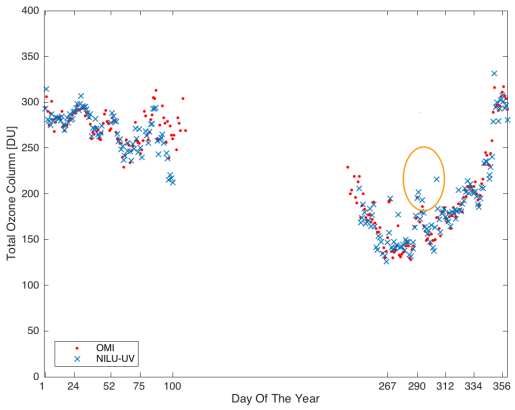

d. TOC peak in 2011.

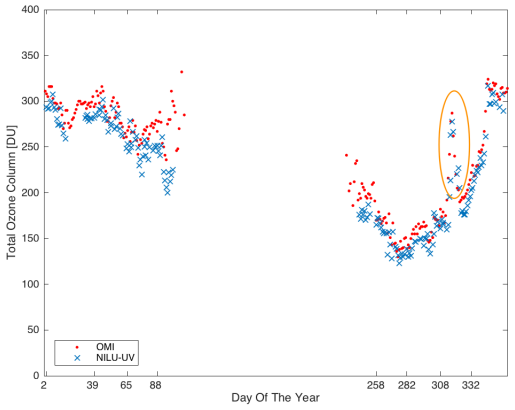

e. TOC peak in 2014.

8. Conclusions

One of the main conclusions of this study is that the NILU-UV instruments deployed at this extreme location in Antarctica provide TOC amounts that correlate well with the results obtained by the OMI. Since both NILU-UV and OMI measurements are affected by clouds in as yet unquantified amounts, it is unclear which instrument (NILU-UV or OMI) provides the most reliable results in the presence of clouds. The effect of growing differences between the measured TOC amounts of ground-based and satellite sensors at higher latitudes, mentioned at the end of Section 6 is also yet to be determined.

NILU-UV results for the ozone hole period correlated well with results from OMI, Halley and TOMS measurements (see Fig. 4). It appears that the NILU-UV instruments deployed at Troll Research Station are suitable for monitoring the long-term change and development of the ozone hole above this station in Antarctica. Because of the large footprint and low measurement time resolution (once a day) of OMI, NILU-UV is a more suitable instrument for short or long term, local TOC measurements.

As mentioned above, ground-based measurements are highly important in addition to satellite

remote sensing monitoring. The magnitudes and fluctuations of the TOC values in the ozone hole region are clearly discernible from the data (Figures and Tables) presented in this paper. Overall the NILU-UV instruments deployed at the Troll station in Antarctica provided reliable results comparable to those obtained from the OMI.

9. Appendix

Figures 10 through 14 show TOC values from OMI (red dots) and NILU-UV (blue asterisks) vs day of the year (DOY) for years 2009, 2012 as well as 2016, 2017 and 2018.

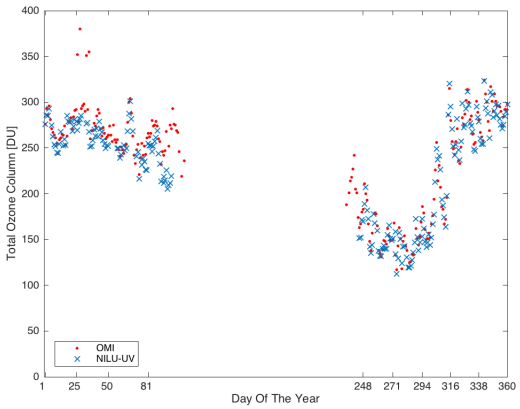

Fig. 10: TOC values from OMI (red dots) and NILU-UV (blue asterisks) vs day of the year (DOY) for 2009.

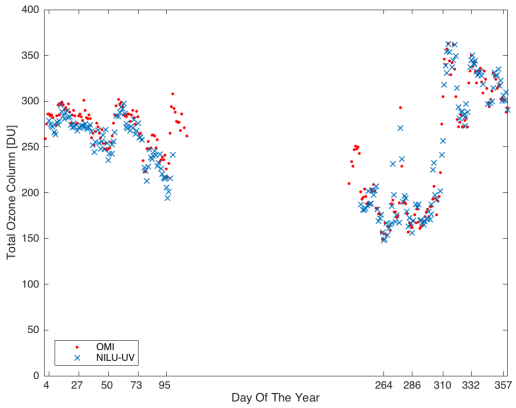

Fig. 11: TOC values from OMI (red dots) and NILU-UV (blue asterisks) vs day of the year (DOY) for 2012.

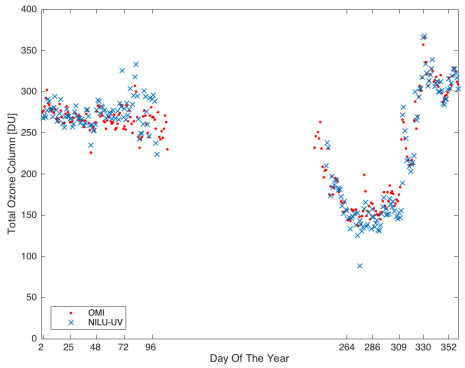

Fig. 12: TOC values from OMI (red dots) and NILU-UV (blue asterisks) vs day of the year (DOY) for 2016.

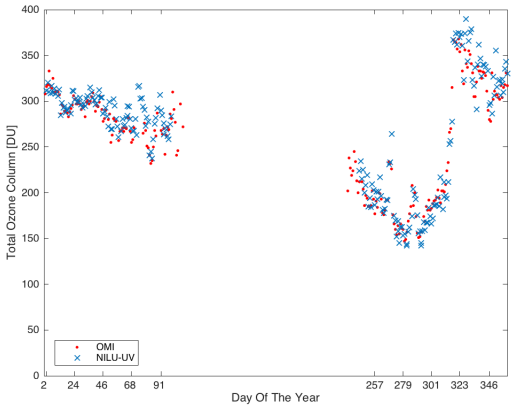

Fig. 13: TOC values from OMI (red dots) and NILU-UV (blue asterisks) vs day of the year (DOY) for 2011.

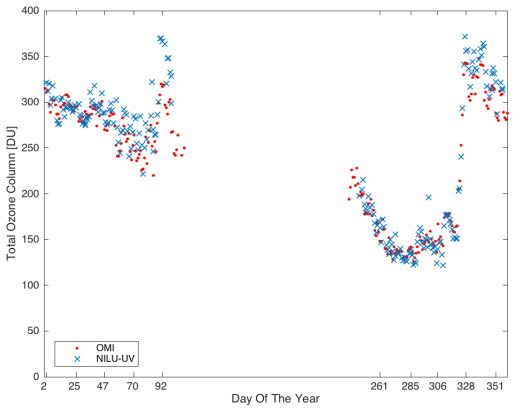

Fig. 14: TOC values from OMI (red dots) and NILU-UV (blue asterisks) vs day of the year (DOY) for 2018.

10. Acknowledgment

The NILU-UV measurements at Troll/Trollhaugen have been financed by the Norwegian Ministry of Climate and Environment. Technical personnel from the Norwegian Polar Institute are responsible for daily maintenance of the instrument.

11. Disclosures

The authors declare no conflicts of interest.

References

1. B. L. Diffey, "Solar ultraviolet radiation effects on biological systems," Phys. Medicine Biol. **36**, 299–328 (1991).
2. T. J. Wang, M. J. Pencina, S. L. Booth, P. F. Jacques, E. Ingelsson, K. Lanier, E. J. Benjamin, R. B. D. Agostino, M. Wolf, , and R. S. Vasan, "Vitamin d deficiency and risk of cardiovascular disease, "circulation"," Phys. Medicine Biol. **117**, 503–511 (2008).
3. J. A. Parrish, K. F. Jaenicke, and R. R. Anderson, "Erythema and melanogenesis action spectra of normal human skin *," Photochem. Photobiol. **36**, 187–191 (1982).
4. Clydesdale, G. J, Dandie, G. W, Muller, and H. Konrad, "Ultraviolet light induced injury: Immunological and inflammatory effects," Immunol. & Cell Biol. **79**, 547–568 (2001).
5. G. Horneck, "Quantification of biologically effective environmental uv irradiance," Adv. Space Res. **26**, 1983 – 1994 (2000).
6. R. M. Lucas and A.-L. Ponsonby, "Ultraviolet radiation and health: friend and foe," Med. J. Aust. **177**, 594–598 (2002).
7. S. Mouret, A. Forestier, and T. Douki, "The specificity of uva-induced dna damage in human melanocytes," Photochem. Photobiol. Sci. **11**, 155–162 (2012).
8. https://ozonewatch.gsfc.nasa.gov/facts/history_SH.html.
9. P. K. Bhartia and R. D. McPeters, "The discovery of the antarctic ozone hole," Comptes Rendus Geosci. **350**, 335 – 340 (2018). 30th Anniversary of the Montreal Protocol: From the safeguard of the ozone layer to the protection of the Earth Climate.
10. https://ozonewatch.gsfc.nasa.gov/facts/images/halley_toms_ozone.png.
11. https://aura.gsfc.nasa.gov/scinst.html.
12. A. Dahlback, "Measurements of biologically effective uv doses, total ozone abundances, and cloud effects with multichannel, moderate bandwidth filter instruments," Appl. Opt. **35**, 6514–6521 (1996).
13. K. Stamnes, G. E. Thomas, and J. J. Stamnes, *Radiative Transfer in the Atmosphere and Ocean* (Cambridge University, 2017).
14. B. A. K. Høiskar, R. Haugen, T. Danielsen, A. Kylling, K. Edvardsen, A. Dahlback, B. Johnsen, M. Blumthaler, and J. Schreder, "Multichannel moderate-bandwidth filter instrument for measurement of the ozone-column amount, cloud transmittance, and ultraviolet dose rates," Appl. Opt. **42**, 3472–3479 (2003).

15. K. Stamnes, J. Slusser, and M. Bowen, "Derivation of total ozone abundance and cloud effects from spectral irradiance measurements," Appl. Opt. **30**, 4418–4426 (1991).
16. P.F. Levelt, G.H.J. van den Oord, E. Hilsenrath, G.W Leppelmeier, P.K. Bhartia, "Algorithm Theoretical Basis Documents Volulme III Chapter 5;," https://www.osapublishing.org. Version 2.0, August 2002.
17. https://ozonewatch.gsfc.nasa.gov.
18. A. Dahlback, "uvproex; extended version," December 18, 2002.
19. L. Fan, W. Li, A. Dahlback, J. J. Stamnes, S. Engelhardt, S. Stamnes, and K. Stamnes, "Comparisons of three nilu-uv instruments deployed at the same site in the new york area," Appl. Opt. **53**, 598–3605 (2014).
20. G. Bernhard, C. R. Booth, and R. D. McPeters, "Calculation of total column ozone from global uv spectra at high latitudes," J. Geophys. Res. Atmospheres **108**, 4532–4543 (2003).
21. A. Kazantzidis, A. F. Bais, M. M. Zempila, C. Meleti, K. Eleftheratos, and C. S. Zerefos, "Evaluation of ozone column measurements over greece with nilu-uv multi-channel radiometers," Int. J. Remote. Sens. **30**, 4273–4281 (2009).
22. https://ozonewatch.gsfc.nasa.gov/facts/hole_SH.html.
23. J.-C. Lambert, M. Van Roozendael, M. De MaziÃĺre, P. C. Simon, J.-P. Pommereau, F. Goutail, A. Sarkissian, and J. F. Gleason, "Investigation of pole-to-pole performances of spaceborne atmospheric chemistry sensors with the ndsc," J. Atmospheric Sci. **56**, 176–193 (1999).
24. https://ozonewatch.gsfc.nasa.gov/monthly/monthly_2008-11_SH.html.